Supplement Section

Supplement Section S.1 Fault outcrop

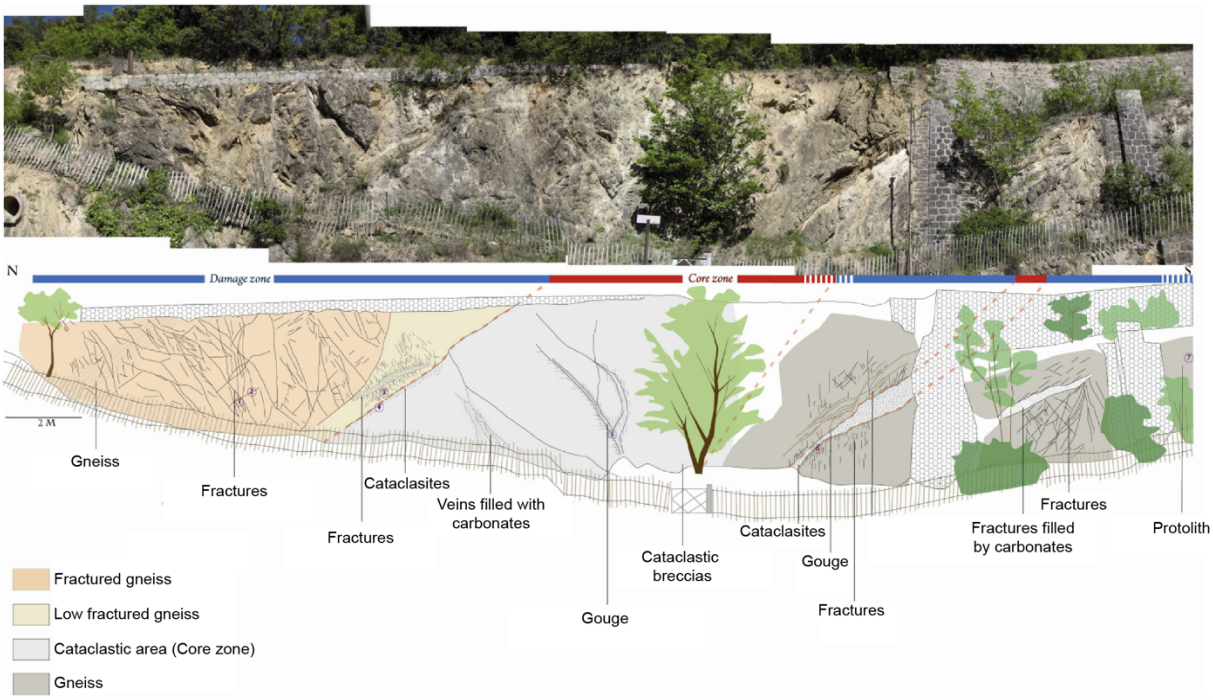

Figure 1. Photo of the Têt fault at Thuès-les-Bains station with interpretation of the fault zone below where Core Zone and Damage zone are distinguished (modified from Martin, 2014). We can see lenses of gneiss preserved near the fault contact and in the damage zone close to the fault.

Supplement Section S.2 Hot spring water analyses

Table 1. Anion et cation composition of hydrothermal hot springs (ST and PB: Saint-Thomas les bains hot spring cluster, TB and CA: Thuès hot spring cluster, VB: Vernet-les-bains,). In bold, data for water potentially mixed with meteoric water from the St-Louis hot spring in Thuès-les-bains hot spring cluster (from Taillefer, 2017).

Cluster		Llo	ST		PB	TB			VB		Ca.
		Llo	Gd Source	Bar.1	Aig.1	St-Louis	Casc. Amont	Casc. Bas	Du Parc	Vap.	Gr. A - Riv.
Ca	mg/l	2.3	1.5	1.4	1.5	**10.1**	1.7	1.5	1.5	3	1.4
Mg	mg/l	<0.5	<0.5	<0.5	<0.5	**0.7**	<0.5	<0.5	<0.5	<0.5	<0.5
Na	mg/l	65.4	55.3	56.4	57	45.8	60.3	60.5	57.2	55.2	60.9
K	mg/l	1.8	1.4	1.3	1.5	1.8	2.4	2.3	1.8	1.9	2.3
NH_4	mg/l	0.25	0.29	0.32	0.33	**<0.05**	0.3	0.29	0.2	0.12	0.29
CO_3	mg/l	21	30	30	33	**<10**	29	30	25	20	33
HCO_3	mg/l	29	27	31	29	**91**	34	32	39	45	31
Cl	mg/l	6.8	8.9	9.2	9.3	8.7	10	9.9	8.4	8.1	7.9
NO_3	mg/l	<0.5	<0.5	<0.5	<0.5	**0.5**	<0.5	<0.5	<0.5	<0.5	<0.5
SO_4	mg/l	51	25.8	25.7	25.7	36.1	28.7	28.3	27.4	37.2	29.5
PO_4	mg/l	<0.05	<0.05	<0.05	<0.05	<0.05	<0.05	<0.05	<0.05	<0.05	<0.05
NO_2	mg/l	<0.01	<0.01	<0.01	<0.01	<0.01	<0.01	<0.01	<0.01	<0.01	<0.01
F	mg/l	17.5	7.4	7.7	7.8	5.3	7.9	7.9	6.9	6.7	7
Ag	$\mu g\,l^{-1}$	<0.01	<0.01	<0.01	<0.01	<0.01	<0.01	<0.01	<0.01	<0.01	<0.01
Al	$\mu g\,l^{-1}$	6.53	23.5	18.2	24.3	6.15	39.5	60.2	21.3	14.1	31.4
As	$\mu g\,l^{-1}$	0.07	6.41	5.77	6.6	5.83	3.42	3.67	0.34	1.66	5.78
B	$\mu g\,l^{-1}$	96.3	109	107	124	221	272	293	301	305	157
Ba	$\mu g\,l^{-1}$	21.4	12.6	22.3	86.6	6.05	40.2	109	67.5	153	143
Be	$\mu g\,l^{-1}$	0.01	0.01	<0.01	<0.01	0.04	0.1	<0.01	<0.01	<0.01	<0.01
Cd	$\mu g\,l^{-1}$	0.01	<0.01	<0.01	<0.01	<0.01	<0.01	<0.01	<0.01	<0.01	<0.01
Cr	$\mu g\,l^{-1}$	<0.05	<0.05	<0.05	<0.05	<0.05	<0.05	<0.05	<0.05	<0.05	<0.05
Cu	$\mu g\,l^{-1}$	<0.1	<0.1	<0.1	<0.1	0.7	<0.1	<0.1	<0.1	<0.1	<0.1
Fe	$\mu g\,l^{-1}$	<0.02	<0.02	<0.02	<0.02	<0.02	<0.02	<0.02	<0.02	<0.02	<0.02
Li	$\mu g\,l^{-1}$	95.3	78	80.1	81.3	71.1	87.7	87.7	69.5	75	93.9
Mn	$\mu g\,l^{-1}$	0.15	0.11	<0.1	<0.1	0.1	<0.1	<0.1	<0.1	<0.1	<0.1
Ni	$\mu g\,l^{-1}$	<0.1	<0.1	<0.1	<0.1	<0.1	<0.1	<0.1	<0.1	<0.1	<0.1
Pb	$\mu g\,l^{-1}$	<0.05	<0.05	<0.05	<0.05	0.2	<0.05	<0.05	<0.05	<0.05	<0.05
SiO_2	$\mu g\,l^{-1}$	55.6	75.3	72.3	79.1	71.8	92.2	92.7	72.7	70.2	91.2
Sr	$\mu g\,l^{-1}$	67	21.9	25.8	20.5	57.8	29.8	28.8	43	75.9	31.9
Zn	$\mu g\,l^{-1}$	0.87	1.91	1.32	3.53	3.19	1.5	2.65	1.51	2.98	2.86

Supplement Section S.3 Apatite grains

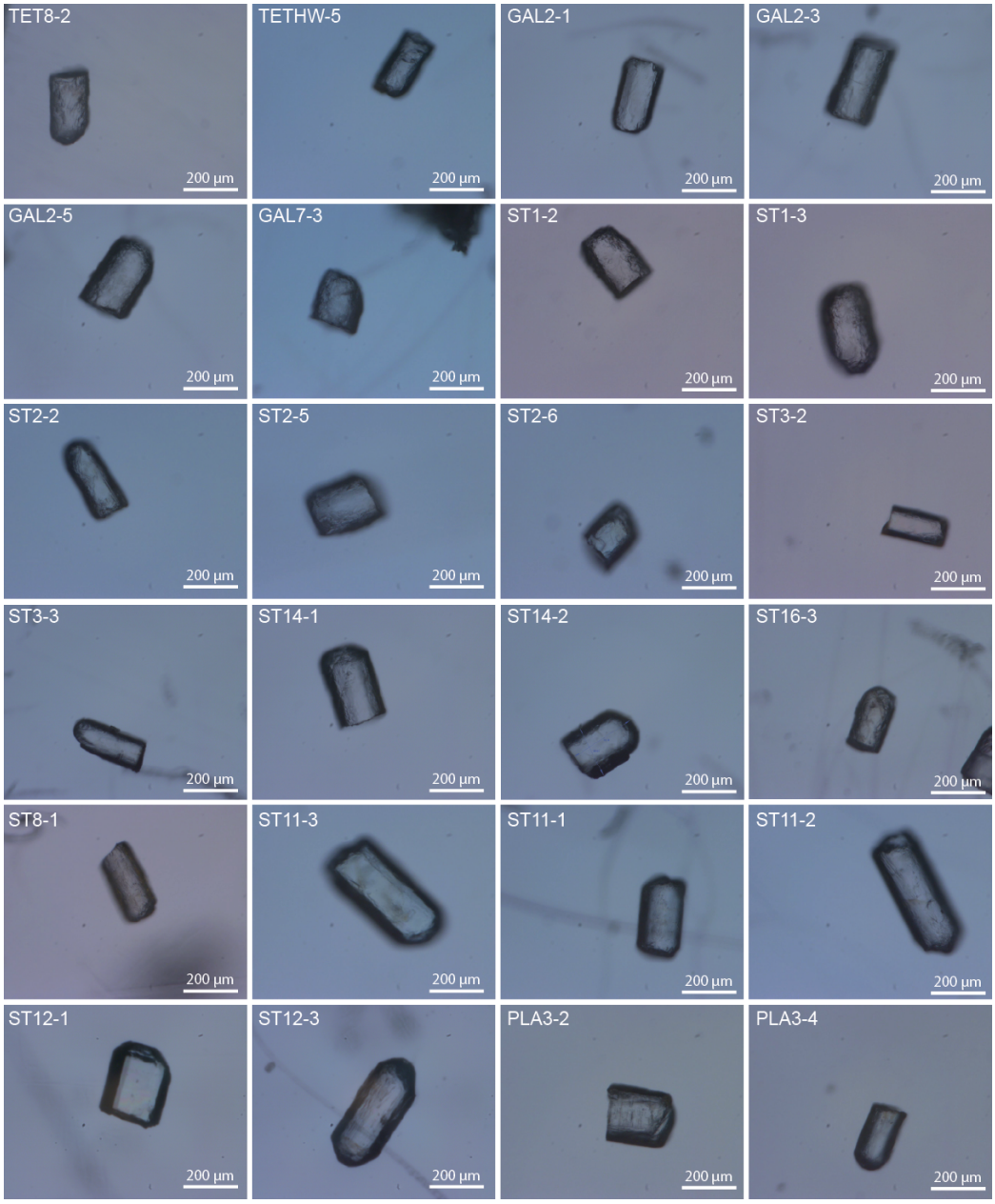

Figure 2. Photographs of apatite grains selected for (U-Th)/He analyses taken under binocular. Sample name is indicated on the upper left corner. Note that apatites are basically well preserved in the damage zone and outside damage zone.

Supplement Section S.4 REE analyses

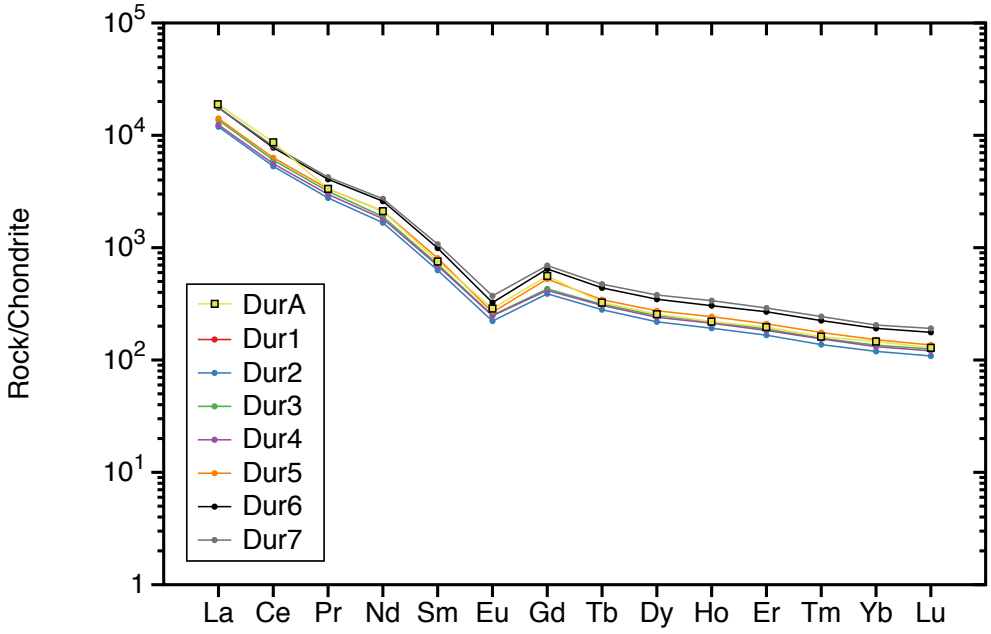

Figure 3. REE patterns for Durango apatite standards, consistent with DurA analysis of Chew et al. (2016).

Table 2. Chondrite normalised REE content of dated apatite grains according to Sun and McDonough (1989).

Profil	Name	AHe ages	La	Ce	Pr	Nd	Sm	Eu	Gd	Tb	Dy	Ho	Er	Tm	Yb	Lu	∑REE
Footwall samples																	
	TET1-2	23.2	557.0	756.2	902.2	1048.2	1526.4	132.9	1858.2	1930.7	1744.1	1354.5	1010.9	785.5	585.4	471.0	14663.3
	TET1-3	36.1	744.2	951.5	1106.5	1248.8	1852.8	150.9	2227.8	2287.1	1980.0	1434.9	1030.8	776.8	549.8	444.6	16786.5
	TET1-4	41.2	421.9	571.5	694.8	821.7	1218.2	112.2	1525.8	1543.4	1333.7	986.5	700.1	534.9	387.3	310.5	11162.4
	TET1.1-1	4.0	82.7	110.1	138.3	164.7	249.8	40.7	305.5	306.7	263.7	191.0	137.4	101.2	76.8	61.7	2230.2
	TET1.1-2	2.2	133.9	168.9	206.4	240.8	355.2	58.8	416.4	417.5	359.5	268.5	194.8	150.0	116.6	92.2	3179.3
	TET1.1-4	21.1	284.7	394.7	446.0	499.0	706.1	54.1	819.6	845.0	743.8	549.7	392.3	304.1	238.6	183.0	6460.9
	TET1.1-11	3.4	197.7	262.1	320.7	375.7	555.5	86.1	665.1	656.7	556.2	417.8	316.8	241.6	195.8	155.2	5003.1
	TET1.1-12	1.1	230.9	297.0	361.9	434.0	629.7	93.0	764.9	758.1	672.7	538.5	413.7	318.7	243.3	196.5	5953.0
TET Profile	TET1.1-13	10.6	537.0	671.7	785.5	885.5	1266.6	206.1	1447.7	1460.7	1279.3	1007.2	769.3	623.9	508.4	403.1	11852.2
	TET2.1-1	10.3	122.1	166.4	215.5	269.4	282.1	84.7	269.2	206.1	175.0	156.7	133.4	108.3	93.0	92.5	2374.3
	TET2.1-2	3.1	63.4	87.6	110.3	134.2	163.0	26.4	176.8	151.7	130.4	107.2	81.3	59.2	43.3	39.2	1374.1
	TET2.1-3	0.3	8.5	5.5	3.4	2.5	1.9	0.7	1.2	1.0	1.0	0.9	0.9	1.0	0.9	0.7	30.2
	TET2.1-4	5.6	111.4	137.0	168.8	208.2	216.5	56.7	208.4	170.0	151.5	137.0	121.4	104.8	91.7	86.5	1969.8
	TET2.1-11	5.6	112.0	136.7	173.7	221.5	255.1	77.1	250.6	202.6	178.3	165.7	152.3	135.4	110.0	109.5	2280.5
	TET2.1-12	6.3	142.0	182.7	233.0	301.1	357.4	91.7	365.0	303.5	279.1	263.2	237.8	211.5	188.8	175.8	3332.6
	TET5-2	23.1	386.3	501.6	571.0	632.4	898.7	68.0	1039.7	1057.6	920.0	676.0	486.8	369.9	284.9	222.7	8115.7
	TET5-4	20.7	456.8	590.5	685.9	757.0	1071.9	83.8	1259.4	1319.8	1166.2	870.8	634.2	485.7	377.2	305.0	10064.2
	CAR7-1	11.2	430.4	578.5	696.0	800.6	1130.2	169.8	1323.6	1345.1	1187.9	914.5	686.3	543.6	415.9	339.7	10562.3
CAR sample	CAR7-2	7.6	131.3	178.7	217.5	264.4	383.7	71.4	463.8	454.1	395.3	298.2	216.4	159.6	116.3	93.6	3444.3
	CAR7-3	10.4	199.4	236.7	272.2	315.1	450.3	66.1	523.0	522.8	461.1	350.8	268.4	215.4	174.3	142.6	4198.1
	CAR7-4	12.4	470.0	605.9	714.5	830.7	1149.5	216.5	1379.8	1380.4	1222.3	951.2	719.1	551.9	427.9	354.2	10973.8
	CAR7-5	13.8	285.1	365.2	431.1	506.1	709.7	113.9	828.5	815.1	705.1	534.7	385.0	275.3	192.6	154.8	6302.2
	CAR7-6	14.3	554.3	740.8	868.3	989.4	1427.5	135.3	1645.1	1678.9	1473.2	1146.6	871.5	702.0	579.8	451.9	13264.7
	GAL7-1	10.6	220.6	251.0	285.5	326.8	271.9	105.1	269.8	192.4	164.4	152.8	133.9	121.5	118.5	142.2	2756.5
	GAL7-2	10.0	1011.8	1103.8	1145.6	1188.2	975.3	236.3	863.1	669.5	574.4	527.1	443.3	381.1	330.9	340.6	9790.9
	GAL7-3	10.6	764.1	829.9	848.8	884.5	685.2	271.9	598.0	432.9	370.5	348.0	315.0	285.1	278.7	328.3	7240.9
GAL Profile	GAL7-4	10.1	366.4	419.3	483.2	600.1	929.5	158.4	1564.3	1742.2	1881.8	1912.1	1811.4	1711.3	1604.9	1445.4	16630.3
	GAL3-1	14.1	379.6	412.0	461.7	526.7	447.4	158.1	608.2	387.3	312.9	278.5	202.5	177.5	156.9	171.0	4680.4
	GAL3-2	10.8	246.9	266.0	294.4	339.2	290.0	94.8	409.3	249.8	190.6	165.8	114.3	98.1	78.2	87.2	2924.5
	GAL3-3	8.6	509.8	503.2	521.3	555.0	436.7	141.5	606.8	360.6	282.3	249.2	181.1	158.5	124.6	143.5	4774.2
	GAL3-4	10.6	489.5	486.6	515.7	552.7	425.8	157.6	552.8	350.2	277.9	251.0	176.8	154.2	137.8	149.8	4678.5
	ST15-1	11.2	53.1	68.1	102.2	175.3	457.0	72.3	868.0	1004.0	1097.2	1124.3	1023.5	869.4	741.9	633.6	8289.6
	ST15-2	12.3	169.7	227.9	278.2	332.9	475.1	47.3	528.2	501.4	429.4	340.5	267.4	241.8	226.5	186.3	4252.5
	ST16-1	12.5	187.5	256.9	324.3	388.9	606.7	56.6	700.4	699.8	603.8	458.0	339.8	265.8	211.0	169.6	5269.2
	ST16-2	15.2	271.8	386.3	488.9	588.8	915.8	86.0	1033.3	1050.3	923.9	701.9	535.0	431.3	342.0	266.4	8021.8
	ST16-3	15.2	343.7	475.2	593.5	730.1	1051.0	103.5	1170.7	1154.3	1038.1	835.6	668.3	590.9	551.2	457.0	9763.0
	ST2-1	16.4	269.6	348.1	409.8	470.1	642.4	78.3	652.4	647.4	590.9	483.4	400.1	334.0	279.8	218.3	5824.5
	ST2-2	14.8	494.6	665.4	835.2	986.8	1329.4	141.1	1336.4	1304.8	1203.7	1025.4	850.2	727.8	594.2	467.6	11962.7
	ST2-3	12.1	10842.3	5392.9	3483.7	2799.5	2537.9	385.6	2622.7	2579.2	2358.0	1995.0	1625.5	1315.9	1024.6	817.3	39780.0
	ST2-4	9.2	5460.6	2576.3	1552.8	1206.6	937.9	157.4	832.0	776.1	705.8	598.4	509.9	441.9	368.6	293.8	16418.1
	ST2-5	15.7	1015.1	1362.1	1645.6	1864.9	2187.0	227.4	2023.3	1959.1	1832.8	1583.7	1381.4	1238.1	1086.6	872.9	20279.8
ST Profile	ST2-6	16.3	580.1	796.4	979.5	1145.0	1493.5	156.9	1485.7	1429.4	1331.1	1096.1	916.9	798.1	644.9	517.3	13370.9
	ST4-1	16.5	618.8	758.4	862.8	879.4	1342.0	192.0	1541.9	1712.4	1444.7	1026.4	752.7	597.6	461.7	357.9	12548.8
	ST4-2	17.2	1023.6	1228.1	1329.9	1336.5	1997.1	267.0	2346.2	2667.7	2272.9	1645.3	1236.2	997.1	802.4	620.1	19770.2
	ST4-3	16.5	766.7	944.8	1043.3	1044.0	1632.3	212.6	1872.2	2122.5	1788.7	1268.8	927.0	743.9	583.1	450.6	15400.4
	ST4-4	16.2	637.2	774.8	851.9	861.1	1330.7	184.1	1545.3	1714.5	1438.3	1004.2	738.1	583.2	450.6	353.4	12467.4
	ST4-5	20.3	456.3	571.6	637.2	650.7	1026.9	143.3	1169.3	1308.4	1080.3	754.8	542.4	433.2	335.1	260.4	9369.9
	ST8-1	21.6	807.9	1023.9	1190.2	1337.3	2001.9	171.5	2367.9	2489.5	2131.9	1574.5	1143.9	887.7	665.7	522.8	18316.7
	ST8-2	19.8	564.1	776.2	953.8	1097.6	1647.1	124.8	1893.8	1982.3	1715.6	1258.2	911.6	697.4	521.1	401.3	14544.8
	ST8-3	19.4	582.1	780.3	938.4	1072.3	1605.4	161.9	1921.1	2021.5	1800.6	1375.7	1010.7	789.8	619.9	494.6	15174.4
	ST8-4	17.6	1098.0	1445.0	1693.8	1908.8	2822.5	242.5	3386.8	3548.8	3104.3	2300.8	1655.5	1245.5	910.1	712.7	26075.0
	PLA3-1	12.4	352.0	416.8	498.8	602.2	890.7	72.8	1111.4	1151.6	1128.8	998.7	873.3	787.1	692.5	583.6	10160.4
	PLA3-2	12.7	116.2	150.8	196.2	261.5	437.2	34.0	546.3	543.7	519.0	453.7	390.1	347.4	308.0	267.6	4571.9
	PLA3-3	14.8	161.9	202.2	255.3	331.9	531.2	41.2	654.1	660.7	623.8	543.3	462.9	410.4	364.1	313.5	5556.6
PLA Profile	PLA3-4	14.5	299.0	387.3	488.7	626.6	1029.7	78.9	1276.5	1288.5	1231.2	1079.6	921.7	825.6	711.3	622.9	10867.6
																	0.0
	PLA2-1	17.1	727.1	974.0	1180.8	1371.7	2154.7	132.0	2501.2	2523.0	2184.3	1634.0	1202.3	932.2	706.9	569.5	18793.6
	PLA2-2	14.8	443.0	622.2	785.4	958.7	1591.3	112.2	1858.4	1850.5	1562.1	1147.7	835.4	647.3	482.3	384.3	13280.9
	PLA2-3	19.1	586.5	785.7	999.0	1169.5	1779.9	128.4	2146.7	2194.6	1921.6	1458.9	1090.8	842.9	653.9	514.1	16272.6
	PLA2-4	15.7	567.1	791.5	968.9	1143.9	1880.6	102.7	2166.8	2172.5	1844.9	1378.1	1017.4	786.0	612.4	485.4	15918.2
Hanging wall samples																	
	TETHW-1	30.6	1205.0	1631.7	1922.1	2114.4	3082.7	289.3	3293.6	3512.7	3181.1	2575.6	2208.5	1933.4	1553.8	1279.5	29783.5
TET Profile	TETHW-2	23.6	1888.7	2596.6	2880.9	3138.5	4209.5	257.7	4643.5	4916.5	4612.5	3821.7	3130.0	2579.2	1997.7	1640.5	42313.7
	TETHW-4	45.6	1635.0	2210.6	2439.2	2672.4	3321.4	274.8	3762.7	3854.5	3629.6	3110.6	2607.3	2122.9	1625.8	1330.1	34597.0
	TETHW-5	14.8	393.7	473.8	549.2	608.2	855.1	107.7	967.1	986.7	900.3	745.6	621.9	541.9	455.4	361.8	8568.4
	ST1-1	40.3	987.2	1312.9	1455.9	1541.9	2413.5	217.9	2586.1	2845.2	2492.1	1823.4	1424.5	1261.2	1121.6	937.7	22421.1
	ST1-2	32.8	658.7	921.9	1105.4	1235.0	1893.6	173.5	2014.8	2151.2	1856.6	1344.4	1015.2	835.6	681.5	557.6	16444.9
	ST1-3	38.3	1085.1	1432.4	1583.1	1704.6	2501.3	232.0	2683.4	2947.8	2642.4	1995.0	1577.2	1355.8	1153.3	953.5	23846.9
	ST1-4	43.2	683.5	870.8	926.9	959.7	1455.9	136.8	1577.3	1761.0	1573.0	1173.5	924.7	824.5	735.1	617.7	14220.4
	ST11-1	21.2	901.3	1249.4	1611.2	1989.8	2593.5	278.8	3946.7	3761.7	3496.2	2942.2	2004.5	1765.6	1279.2	1239.1	29059.2
ST Profile	ST11-2	24.3	1300.3	1720.1	2150.5	2589.6	3438.7	362.0	5222.7	4921.7	4639.6	3933.2	2720.3	2457.4	2003.9	1780.7	39240.9
	ST11-3	20.2	1163.0	1531.8	1885.1	2289.7	3016.8	291.5	4461.5	4279.1	4014.6	3383.7	2337.1	2075.7	1767.4	1477.4	33974.4
	ST11-5	24.9	880.1	1157.2	1455.7	1814.5	2376.1	249.7	3575.9	3383.5	3181.9	2653.7	1812.1	1577.5	1061.5	1073.3	26252.8
	ST12-1	29.4	189.1	204.0	272.4	399.7	904.3	82.8	1781.0	2021.8	2177.5	2106.8	1632.1	1549.4	1431.5	1247.1	15999.5
	ST12-2	35.2	105.2	122.8	173.5	268.3	680.0	73.1	1433.7	1707.8	1900.3	1886.9	1474.6	1436.4	1345.8	1141.4	13749.8
	ST12-3	29.4	129.1	142.7	193.1	281.4	653.6	65.7	1341.8	1507.2	1644.9	1598.0	1227.4	1172.6	1074.2	945.6	11977.1
	ST12-4	36.8	102.5	110.4	143.2	203.1	486.7	56.3	1016.8	1182.1	1312.0	1293.8	999.2	942.2	866.9	761.1	9476.4
	ST12-5	35.2	273.4	322.0	428.2	618.3	1354.6	120.3	2641.7	2953.8	3153.9	3065.1	2335.9	2244.2	2035.0	1790.2	23336.8
	PLA5-1	23.3	220.5	244.8	302.9	410.7	947.3	77.7	1650.7	1948.7	2117.4	2082.8	1986.7	1868.6	1725.0	1570.4	17154.3
PLA Profile	PLA5-2	41.5	282.1	317.6	396.9	546.7	1186.4	83.4	1978.6	2263.8	2405.8	2362.7	2225.1	2087.0	1913.6	1713.4	19763.1
	PLA5-3	29.9	251.1	269.6	328.3	444.3	1019.5	81.8	1841.1	2137.2	2299.5	2282.2	2166.8	2028.8	1834.9	1667.5	18652.6
	PLA5-4	37.5	1337.9	1340.4	1281.1	1111.6	1237.0	78.1	1077.1	1385.0	1505.7	1412.1	1379.8	1423.1	1415.4	1242.8	17227.2

REE analyses were performed at Géosciences Montpellier using the equipment available at the AETE-ISO analytical platform of the OSU OREME (University of Montpellier)

Supplement Section S.5 Chemical analyses of apatite

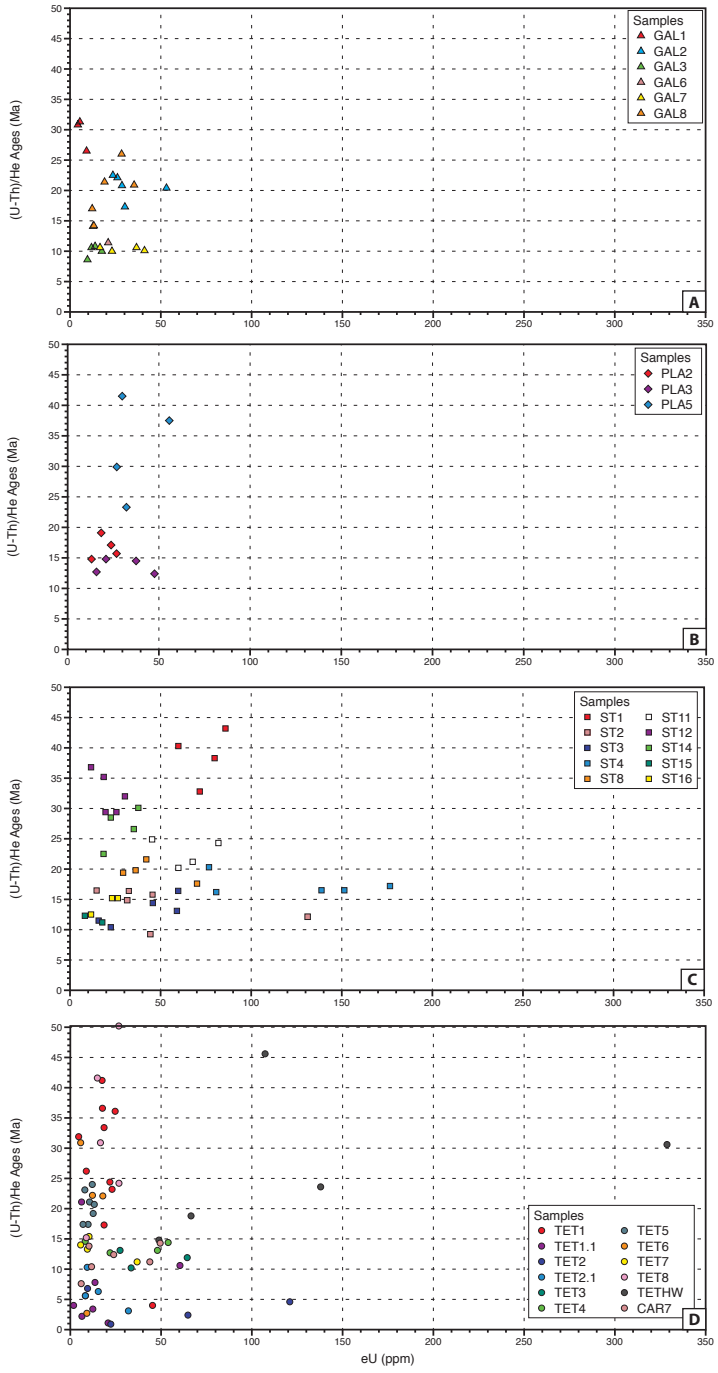

Figure 4. (U-Th)/He ages vs. eU (U+0.235*Th) for the 4 different profiles: A) Thuès B) Galinàs C) St-Thomas D) Planès.

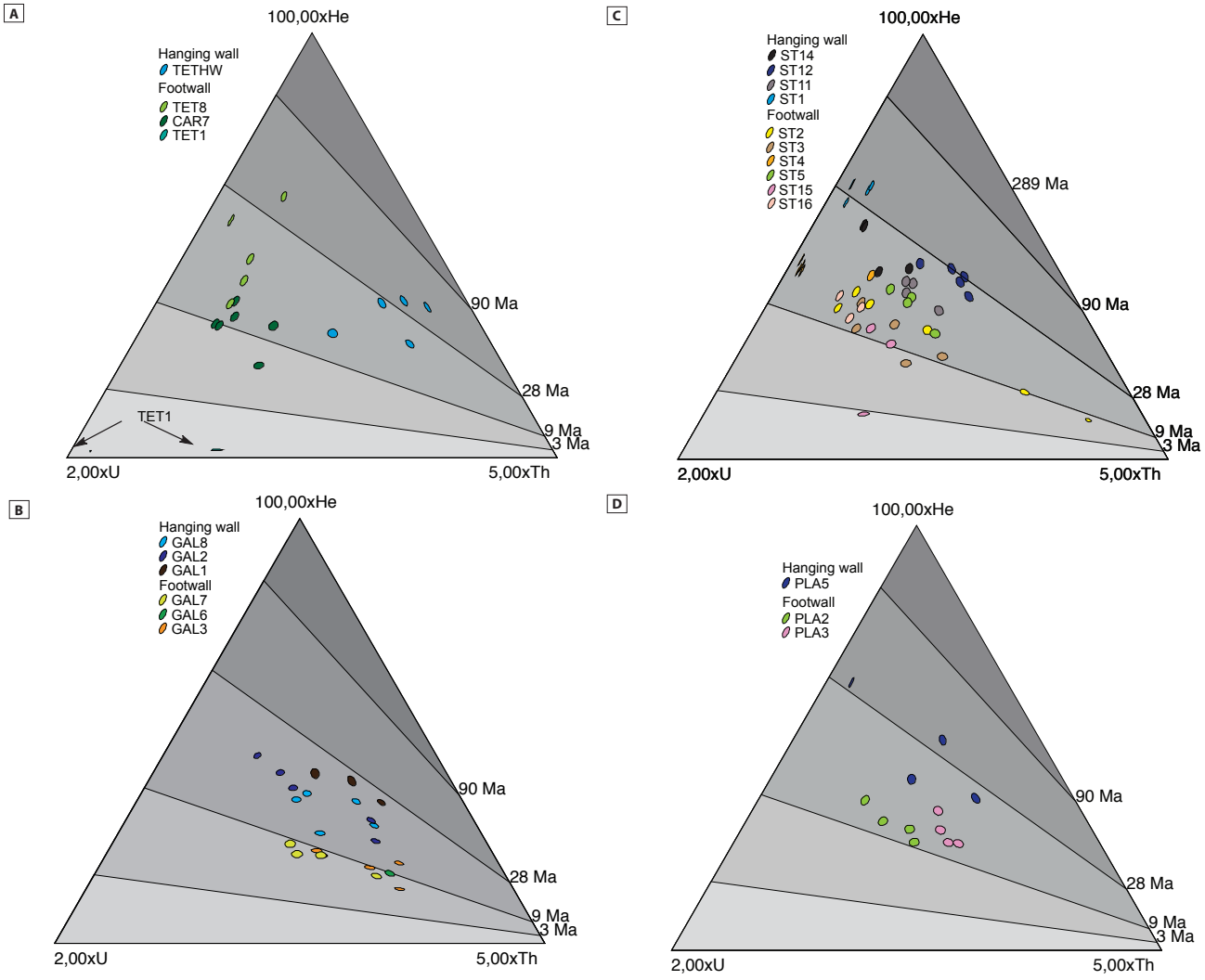

Figure 5. U-Th-He ternary diagrams using Helioplot (Vermeesch, 2010) for the 4 profiles where samples from the Têt fault footwall and hanging wall are distinguished A) Thuès B) Gallinàs C) St-Thomas D) Planès.

Supplement Section S.6 Numerical modelling under QTQt

Table 3. QTQt models parameters for the Têt fault footwall and hanging wall.

QTQt model for the Têt fault footwall
Samples and data used in simulations
AHe data
TET3
TET4
TET5
TET7
GAL3
GAL6
GAL7
AFT data (Maurel et al., 2008)
ZHe data (Maurel et al., 2008)
Data treatment, uncertainties, and other relevant constraints
AHe data
Treatment: Each of the 4 samples was used as a separate constraint in QTQt. Uncorrecte
He ages (Ma): Uncorrected He age of each apatite grain
Error (Ma) applied in modelling: the 1σ sample standard deviation
r (µm): equivalent radius of each apatite grain
eU (ppm): eU of each apatite grain
eU zonation: none
Additional geologic information
Assumption
At surface temperature of 15 ± 10°C by 0 Ma
Motion of Canigou and Carança massif
System and model specific parameters
He kinetic model: Gautheron et al. (2009)
Modelling code: QTQt v.5.7.0
Number of MCMC chain 100000

QTQt model for the Têt fault hanging wall
Samples and data used in simulations
AHe data
ML1
ST14
ST12
GAL2
GAL1
AFT data (Maurel et al., 2008)
ZHe data (Maurel et al., 2008)
Data treatment, uncertainties, and other relevant constraints
AHe data
Treatment: Each of the 4 samples was used as a separate constraint in QTQt. Uncorrecte
He ages (Ma): Uncorrected He age of each apatite grain
Error (Ma) applied in modelling: the 1σ sample standard deviation
r (µm): equivalent radius of each apatite grain
eU (ppm): eU of each apatite grain
eU zonation: none
Additional geologic information
Assumption
At surface temperature of 15 ± 10°C by 0 Ma
Motion of Mont Louis massif
System and model specific parameters
He kinetic model: Gautheron et al. (2009)
Modelling code: QTQt v.5.7.0
Number of MCMC chain 100000

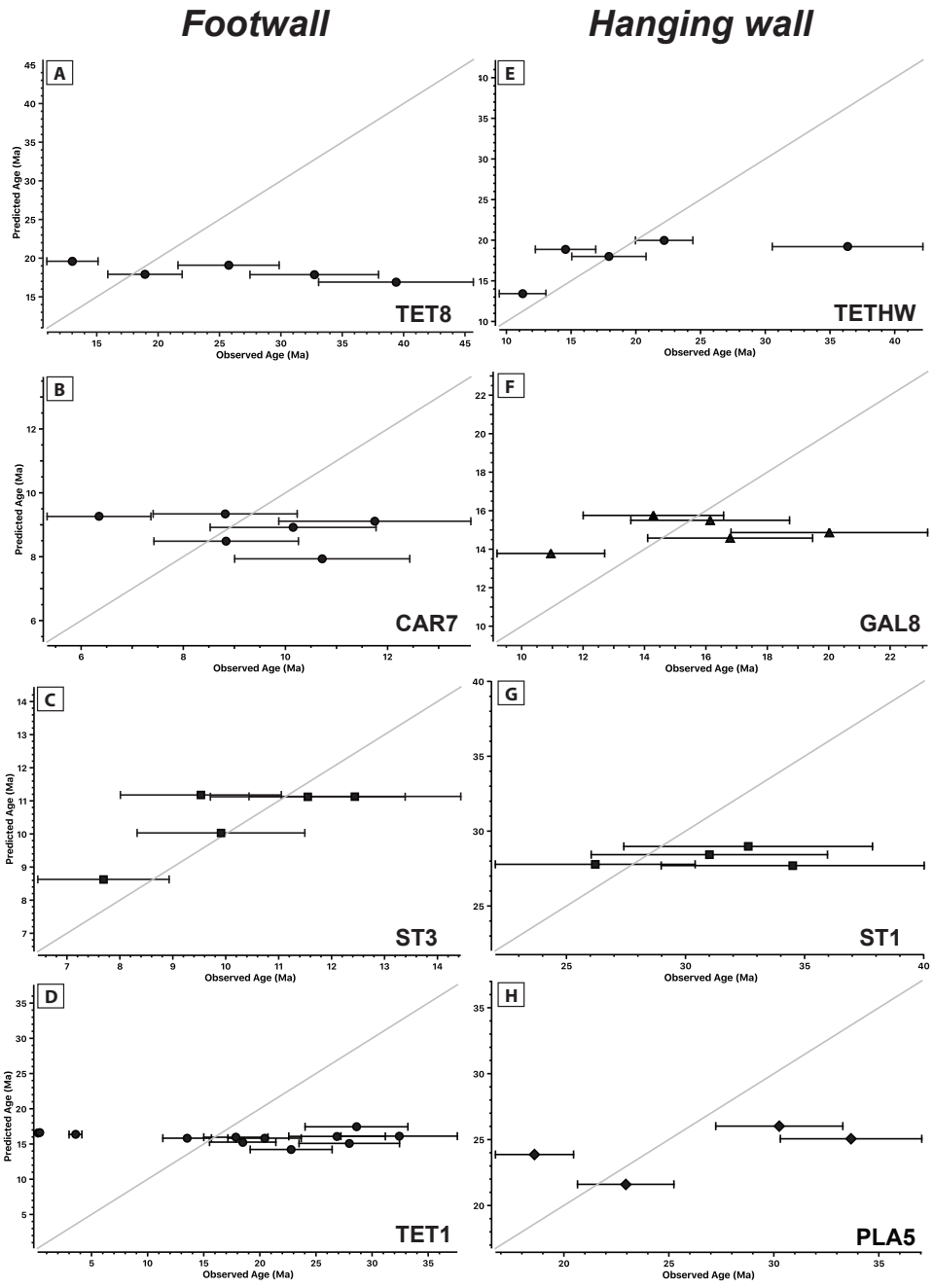

Figure 6. Predicted age vs Observed age graph using QTQt (Gallagher, 2012) for samples from the damage zone footwall (A,B,C and D) and hanging wall (E,F,G and H), computed with Gautheron et al. (2009) diffusion model. Modelling parameters are those of Table 3 with AFT and ZHe data from Maurel et al. (2008). For all samples, the weak or the lack of correspondence between observed and predicted ages indicates that no regional cooling history can reasonably explain the AHe age dispersion.

References

Chew, D. M., Babechuk, M. G., Cogné, N., Mark, C., O'Sullivan, G. J., Henrichs, I. A., Doepke, D. and McKenna, C. A.: (LA,Q)-ICPMS trace-element analyses of Durango and McClure Mountain apatite and implications for making natural LA-ICPMS mineral standards, Chemical Geology, 435, 35–48, doi:10.1016/j.chemgeo.2016.03.028, 2016.

Gallagher, K.: Transdimensional inverse thermal history modeling for quantitative thermochronology, Journal of Geophysical Research: Solid Earth, 117(B2), n/a-n/a, doi:10.1029/2011JB008825, 2012.

Gautheron, C., Tassan-Got, L., Barbarand, J. and Pagel, M.: Effect of alpha-damage annealing on apatite (U–Th)/He thermochronology, Chemical Geology, 266(3–4), 157–170, doi:10.1016/j.chemgeo.2009.06.001, 2009.

Martin G. : Analyse des relations entre structure de la faille de la Têt et sources hydrothermales. MSc Thesis, Montpellier, 45, 2014.

Maurel, O., Monié, P., Pik, R., Arnaud, N., Brunel, M. and Jolivet, M.: The Meso-Cenozoic thermo-tectonic evolution of the Eastern Pyrenees: an 40Ar/39Ar fission track and (U–Th)/He thermochronological study of the Canigou and Mont-Louis massifs, International Journal of Earth Sciences, 97(3), 565–584, doi:10.1007/s00531-007-0179-x, 2008.

Sun, S. S., and McDonough, W. F.: Chemical and isotopic systematics of oceanic basalts: implications for mantle composition and processes. Geological Society, London, Special Publications, 42p, 313–345. https ://doi.org/10.1144/GSL.SP.1989.042.01.19, 1989.

Taillefer, A.: Interactions entre tectonique et hydrothermalisme : Rôle de la faille normale de la Têt sur la circulation hydrothermale et la distribution des sources thermales des Pyrénées Orientales., Thesis, Montpellier, Montpellier, 27 October., 242p , 2017.

Vermeesch, P.: HelioPlot, and the treatment of overdispersed (U–Th–Sm)/He data, Chemical Geology, 271(3–4), 108–111, doi:10.1016/j.chemgeo.2010.01.002, 2010.